This is a repository copy of *Pore system characteristics of soil aggregates and their relevance to aggregate stability*.

White Rose Research Online URL for this paper:
http://eprints.whiterose.ac.uk/157758/

Version: Accepted Version

Article:
Menon, M. orcid.org/0000-0001-5665-7464, Mawodza, T., Rabbani, A. et al. (6 more authors) (2020) Pore system characteristics of soil aggregates and their relevance to aggregate stability. Geoderma, 366. 114259. ISSN 0016-7061

https://doi.org/10.1016/j.geoderma.2020.114259

Article available under the terms of the CC-BY-NC-ND licence (https://creativecommons.org/licenses/by-nc-nd/4.0/).

Reuse
This article is distributed under the terms of the Creative Commons Attribution-NonCommercial-NoDerivs (CC BY-NC-ND) licence. This licence only allows you to download this work and share it with others as long as you credit the authors, but you can't change the article in any way or use it commercially. More information and the full terms of the licence here: https://creativecommons.org/licenses/

Takedown
If you consider content in White Rose Research Online to be in breach of UK law, please notify us by emailing eprints@whiterose.ac.uk including the URL of the record and the reason for the withdrawal request.

eprints@whiterose.ac.uk
https://eprints.whiterose.ac.uk/

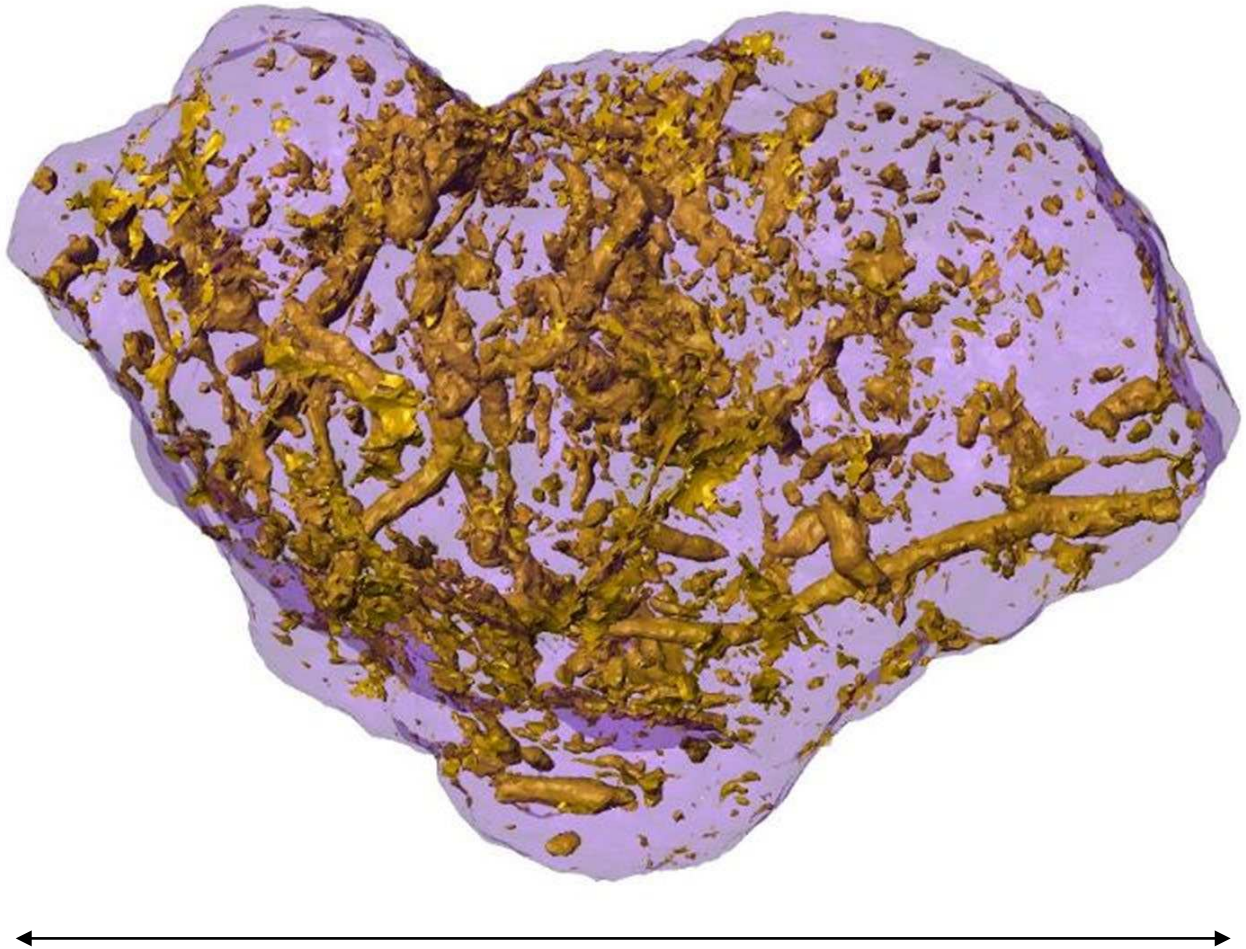

A 3D view of the pore system of a ~5 mm size aggregate grassland aggregate using X-ray microtomography at 5µm resolution. The pores are given in yellowish brown in the purple coloured aggregate solid matrix. This paper aims to characterise and quantify the pores in aggregates and establish its relevance to aggregate stability.

Running title: Aggregate pores and stability

Pore system characteristics of soil aggregates and their relevance to aggregate stability

Manoj Menon[1@], Tinashe Mawodza[1,] Arash Rabbani[2], Aimeric Blaud[1,3], Georg. J. Lair[4], Masoud. Babaei[2], Milena Kercheva[5], Svetala Rousseva[5] And Steven Banwart[1,6*]

[1] The University of Sheffield, Western Bank, United Kingdom, S10 2TN

[Email: m.menon@sheffield.ac.uk; tmawodza@sheffield.ac.uk]

[2] School of Chemical Engineering and Analytical Science, The University of Manchester, Manchester, United Kingdom, M13 9PL.

[Email: arash.rabbani@postgrad.manchester.ac.uk; masoud.babaei@manchester.ac.uk]

[3*] School of Applied Sciences, Edinburgh Napier University, Sighthill campus, Edinburgh, United Kingdom, EH11 4BN.

[Email: aimeric.blaud@rothamsted.ac.uk]

[4] University of Natural Resources and Life Sciences (BOKU), Institute of Soil Research, Vienna, Peter-Jordan-Str. 82, 1190, Vienna, Austria.

[Email: georg.lair@tirol.gv.at]

[5] Department of Soil Physics, Institute of Soil Science, Agrotechnology and Plant Protection "Nikola Poushkarov" (ISSAPPNP), 7, Shosse Bankya str. 1080 Sofia, Bulgaria

[Email: mkercheva@abv.bg; svetlarousseva@gmail.com]

[6*] Global Food and Environment Institute and School of Earth and Environment, University of Leeds, United Kingdom, LS2 9JT.

[Email: S.A.Banwart@leeds.ac.uk]

*Current address

@ Corresponding Author. Department of Geography, University of Sheffield, Sheffield, United Kingdom, S10 2TN. Email: m.menon@sheffield.ac.uk

Abstract

Aggregates are the structural units of soils, and the physical stability is considered to be a keystone parameter of soil quality. However, little is known about the evolution of the pore system in aggregates and its importance in defining aggregate stability. In this paper, we investigated the pore system and stability of three dominant macroaggregate sizes (1-2, 2-5 5-10 mm) obtained from a fine sand-loamy Chernozem under three distinct land uses (arable, grassland and forest). We used non-invasive X-ray microtomography (XMT) in combination with pore network extraction to characterise PSD (pore size distribution) of aggregates and their potential changes upon continued submergence in water. We showed that smaller aggregates (1-2mm) have significantly higher total X-ray resolvable porosity than the medium (2-5 mm) and large (5-10 mm) aggregates. Also, using imaging tools, we demonstrated for the first time, that the pore system of stable aggregates from grassland and forest does not undergo significant changes upon continued submergence in water. It can be hypothesised that a physically stable pore structure allows the storage and transmission of water without a structural collapse, thereby contributing to aggregate stability. We found statistically significant positive correlations between different pore groups (closed pores, water holding pores and air space spores) and water stability of aggregates from all three land uses suggesting that pore system characteristics play a significant role in aggregate stability. Our results suggest that PSD is an important factor that determines the stability of soil aggregates.

Keywords: Imaging, Land Use, Aggregates, Pore network, Porosity, Tortuosity

Highlights

- The main aim is to establish links between aggregate pore system characteristics and stability.

- We analysed pore systems of macroaggregates from different land use using X-ray microtomography.
- There were no significant changes in the pore system in stable aggregates upon submergence.
- A stable pore system in aggregates is crucial for aggregate stability in water.

1.0 Introduction

Soil structure is a keystone indicator of soil quality, function and health (Kibblewhite et al., 2008). The stability of soil structure reflects the ability of soil to support soil flora and fauna through provision of void space as habitat, and the storage and transfer of water, gas and nutrients in soils (Utomo and Dexter, 1982; Amézketa, 1999; Bronick & Lal, 2005; Rabot et al., 2018; Banwart et al., 2012). In general, soil structure refers to the three-dimensional arrangement of soil voids within and between aggregates of primary soil particles whereby aggregates can be viewed as the structural units of soils. The development of aggregates is explained by the aggregate hierarchy model proposed by Tisdall & Oades (1982). Based on this conceptual model aggregates are sequentially formed through the action of organic (transient, temporary or persistent) binding agents leading to the formation of microaggregates (20-250 μm) and then to macroaggregates (>250 μm). It was also suggested that microaggregates could also be formed within macroaggregates due to the action of roots and microbiota (Oades, 1984) and aggregates also provide physical protection of organic carbon (Six et al., 2004).

Pores within aggregates (intraaggregate pores) can also be regarded as microsites for storage of air, water, nutrients and microbes which create localised pore-scale biogeochemical cycles. In unsaturated soils, all pores between 0.2 and 30μm retain water except the blocked pores with entrapped air (i.e. between -10 kPa and -1.5MPa matric potentials) and pores greater than 30μm in diameter typically filled with air (Dexter, 1988). Dexter (1988) also proposed the porosity exclusion principle, which states that each hierarchical order excludes the pores between the particles of the next higher order. Although this has not been verified experimentally, the theory suggested that smaller aggregates would have a denser packing (or lesser pore space) compared to larger aggregates. However, Lipiec et al. (2007) provided additional insights into the pore space within aggregate beds. In their investigation, they

evaluated individual aggregate beds made of <0.25, 0.25-0.5, 0.5-1, 1-3, 3-5, and 5-10 mm sized aggregates for water retention and pore size distribution (PSD) and found that aggregate beds <1 mm exhibited bi-modal PSD associated with textural and structural domains whereas aggregate beds >1 mm produced tri-model PSD due to the additional macropore domain.

Non-destructive imaging tools such as X-ray microtomography (XMT) provide an alternative method to study PSD aggregates at a few micrometres resolution. For instance, Peth et al. (2008) used a high resolution (3.2-5.4 μm) XMT to image ~5 mm diameter aggregates from different land use (grass and conventionally-tilled). Based on the image analysis carried out using a small region of interest from near the centre of the aggregate, they found that the total porosities were higher for the conventionally-tilled (CT) aggregate (15.7%) compared with the grassland aggregate (11.1%). They also found higher relative proportions of smaller pores are observed in the former compared with the latter. Kravchenko et al (2011) reported that the aggregates under natural succession had more large pores (>97.5 μm) and small pores (<15 μm) than conventionally-tilled aggregates; whereas the medium size pores (37.5-97.5 μm) dominated in conventionally-tilled aggregates (Wang et al., 2012). A study by Zhou et al (2016) compared different fertiliser treatments on aggregate (3-5 mm) porosity in paddy soils using XMT and they found that total porosity of aggregates was higher when no fertiliser was applied in comparison to both fertiliser treatment (inorganic fertiliser with or without organic manure). Recently, (Bacq-Labreuil et al. 2018) showed the effect of land use (vegetation) on aggregates using XMT, and they found the total pore volume was influenced by vegetation as follows: grassland> arable> fallow.

According to Peth et al. (2008), further studies are required to link PSD with other soil properties, and there has been some progress in this direction; for example, Bailey et al. (2013) used imaging to understand the relationship between the porosity of 14 grassland aggregates of different sizes (0.250-0.425, 0.425-0.841, 0.841-1.0 mm) and microbial

112 community composition and found no correlation between them. Similarly, the relationship
113 between the aggregate PSD and stability was investigated by a few researchers. Soil structure
114 stability is classically described by the mass distribution by particle size class of water stable
115 aggregates (WSA as %) present in a soil sample. Note that several organic and inorganic
116 binding agents contribute to the development of WSA (Tisdall & Oades, 1982; Amézketa,
117 1999; Bronick & Lal, 2005; Dal Ferro et al., 2012; Regelink et al., 2015; Rabot et al., 2018).
118 Papadopoulos et al. (2009) examined 5 mm sized aggregates using XMT and found that
119 aggregate porosity was not linked to stability; however, the authors reported that pore
120 morphology might influence the stability of aggregates and the potential for slaking (i.e. the
121 breakdown of macro-aggregates to microaggregates and primary textural units). However,
122 using 1-2 mm sized aggregates Dal Ferro et al. (2012) established that aggregate stabilisation
123 was strongly linked to the porosity.

124 If an aggregate is considered water stable, it must withstand the decrease in inter-particle
125 cohesive forces within the aggregate imparted by wetting without a structural collapse
126 through slaking, clay swelling or clay dispersion (Dexter, 1988). Conceptually, the presence
127 of a stable macropore domain (including cracks and elongated pores) within aggregates may
128 prevent trapping of air or build-up of air pressure in pores due to the entry of water. These
129 stable pores may play an important role in transmitting water without disrupting the structure
130 of aggregates and therefore could contribute to the stability of the aggregates (Lipiec et al.,
131 2007; Papadopoulos et al., 2009). In other words, in a stable water aggregate, the macropore
132 domain may remain stable when it is subjected to wetting, thus contributing to the stability.
133 However, this concept requires experimental validation. Therefore, in this paper, we would
134 like to test three important hypotheses, which are linked to pore system development in
135 macroaggregates and their linkages to aggregate stability as below:

(1) The total XMT resolvable pore space in macroaggregates will increase with an increase in the size of the aggregates according to the porosity exclusion principle.
(2) Aggregates from less disturbed land use (e.g. grassland and forest) will have greater total porosity dominated by macropores compared to disturbed land use (e.g. arable).
(3) Stable aggregates will have a pore system that is resilient to changes during wetting.

The specific objectives are:

1. Describe XMT resolvable PSD in three different macroaggregate sizes (1-2; 2-5 and 5-10 mm) obtained from three different land uses (arable, grassland and forest) using XMT;
2. Examine the stability of aggregates during rigorous wetting regimes;
3. Evaluate the XMT resolvable PSD changes in stable aggregates before and after wetting

2.0 Methods

2.1 Site description and sampling

The samples were obtained from locations in the National Park Donau-Auen, which were developed on fine river sediments of the Danube River and part of the FM-CZO. The mean annual temperature in the area is about 9°C and mean annual precipitation ~550 mm with potential evapotranspiration of ~570 mm (Blaud et al., 2018). The soil is a fine sandy-loamy Haplic Chernozem (Mollic Fluvisols as per WRB) soils that are ~350 years old (Lair et al., 2009). Three contrasting land uses (arable, grassland and forest) were selected for soil sampling. The bulk soils characteristics at the time of sampling are given in Table 1, and

more information about the site can be found in other references (Banwart et al., 2012; Regelink et al., 2015; Rousseva et al., 2017; van Leeuwen et al., 2017).

Aggregate sampling was carried in summer 2011 under dry soil conditions (pF 3.8 - 4.0) which enabled sieving and collection of aggregates in the field. Three sample locations were chosen as replicates within 30 m radius under each land use. The top 5 cm of the soil profile was scraped off to remove the surface leaf litter, earthworm castings and surface feeding roots in grassland and forest. The soil beneath (5-10cm) was then loosened using a spade and passed through a stack of sterilised sieves to collect different aggregate size classes (<0.25, 0.25-0.50, 1-2, 2-5 and 5-10mm) for various experiments including microbial diversity studies (e.g. Blaud et al., 2018). The soil aggregates were stored in plastic beakers and kept dry in the dark and cold room conditions (4ºC) for subsequent use. However, for this study, we used three dominant macroaggregate sizes which were 1-2, 2-5 and 5-10mm (see Table 1 for particle size distribution) which will be denoted by S (small), M (medium) and L (large), respectively, in this manuscript.

2.2 Experiments

The experiment included imaging of dry sieved aggregates collected from the field, followed using three wetting and drying cycles on major aggregate size fractions (S, M and L). Based on the water stability tests, we tested the effect of submergence on aggregates PSD through imaging as described below.

2.2.1 Microstructure measurements using XMT

Sixty-nine aggregates were scanned representing each size class (7 from S; 8 from M and L) from the three land uses. We used Skyscan 1172 XMT scanner available at the SKELETAL lab at the University of Sheffield with an effective pixel size of 10µm for L size and 5 µm for S and M size aggregates to achieve maximum resolution for a given aggregate size (See

Suppl. Material 1 for image acquisition settings) for this scanner. Individual aggregates were scanned by securely placing in them in Styrofoam (which does not appear in X-ray images) before fixing on the tomography stage to obtain 3D images of aggregates.

2.2.2 Aggregate stability using three wetting and drying cycles (WDC)

This experiment aimed to measure the amount of water stable macroaggregates (WSA) from S, M and L of each land use. The initial macroaggregate WSA (%) was measured using standard wet sieving procedure (method 1) with multiple sieves that were sequential (<0.25, 0.25-0.50, 1-2, 2-5 and 5-10mm) (Elliott, 1986). However, for the WDC experiment, a single 0.25mm sieve (method 2) was used to allow a simple and straightforward separation of water stable macro and microaggregates as both methods showed a strong positive and significant correlation (correlation coefficient= 0.99, not shown). Note that the sand content of the aggregates was checked using ultrasound stability tests (data not shown) before the wet sieving experiments to verify the need for sand correction. It was found that large sand (630-2000µm) and medium sand fractions (200-630µm) were negligible, and ~95% of sand particles were made of fine sand (63-200 µm). Based on this, the sand correction procedure was not followed for macroaggregates fractionation (>250µm).

Exposing aggregates to varying degrees of wetting and drying cycles (WDC) provided a better understanding of the structural resilience of aggregates; however, there is no consensus on number or duration of WDCs (Rabot *et al.*, 2018). Two WDCs were considered for S, M and L sized aggregates from all land use: (1) a short WDC with 2 hours of submergence followed by 22 hours drying at 25-35ºC in a laboratory (i.e. 24 hours per cycle); and (2) a long WDC, in which the aggregates were submerged for 24 hours followed by 24 hours drying (i.e. 48 hours per cycle). The short cycle was repeated four or nine times whereas the

long cycle was repeated for four times only. Three replicates per treatment were used. We performed WSA analysis using method 2, as outlined earlier.

To investigate changes in soil aggregates due to processes such as slaking or expansion of clay, we performed additional imaging of individual aggregates after 24-hour continuous submergence in water to induce slaking. It was assumed that 24 hours were sufficient to fully saturate all pore spaces in aggregates and the water pressure on the pore walls could induce pore system instability and slaking. We used only a subset of three M, and L aggregates each from grassland and forest. In this experiment, selected aggregates were individually placed gently in a sterilised 50 ml beakers, and deionised water was added (~25 ml) along the side of the beakers until the aggregate to be completely submerged. The arable soil aggregates slaked and disintegrated rapidly within seconds after adding water; hence, they could not be included in this investigation. The samples were left for 24 hours in the laboratory conditions with a parafilm lid to prevent evaporation. After this, we syphoned the water out carefully without disturbing the aggregate, and any remaining water was left to dry naturally for approximately two days before imaging. Due to the fewer number of samples and better hardware availability, these aggregate images were processed at the original scanning resolution (5 and 10 µm for M and L) to study the PSD in detail.

2.3 Image processing and pore network extraction.

The working resolution was set at 20µm for L and 10µm for S and M due to a large number of samples and optimum hardware and software (Avizo 9.0.1) performance. All previously reported studies used a region of interest (ROI) while quantifying pore system in aggregates. While this is useful, it only will represent part of an aggregate, and the distribution of pores cannot be assumed spatially uniform throughout in an aggregate. Hence, we developed a new protocol for quantifying the total porosity in a given aggregate volume as described in

228 Supplementary Material 1, largely based on methods described in our previous publication
229 (Menon et al., 2015). In general, the processing steps included image cropping using ImageJ
230 to 8-bit JPEG files to reduce the computational burden of processing images in 3D using
231 Avizo. The pores present after segmentation provided a total porosity of the image in 3D. For
232 the segmentation, the solid particles were isolated using an image thresholding algorithm that
233 uses a specified discrete attenuation value above which all pixels are considered as solid
234 particles. To extract different types of pores from an image, a series of morphological filters
235 were used as described in the Suppl. Material 1.

236 Based on our analysis, the porosity of each aggregate is presented, which is the proportion of
237 total pores to the total volume of the aggregate. Further, we grouped the pores broadly into
238 closed (or isolated air pockets in the structure), pores <50µm (water holding) and >50 µm (air
239 space) to the total pore volume are also presented. Also, effective porosity (%) is presented,
240 which is the proportion of the combined water holding and the air space to the total pore
241 volume of each aggregate. Please note that the amount of resolvable pores in each category
242 will depend on the resolution of the images.

243 The pore space can be segmented into its structural elements, including pores and throats
244 (Dong & Blunt, 2007). Throats are the bottlenecks between each pair of connecting pores
245 (Blunt, 2001). This simplified model allows us to simulate complicated processes in porous
246 media within a computationally efficient framework. Thanks to their applicability and
247 facilitated by computed tomography images, pore networks have been employed to model
248 various porous material processes (Blunt, 2001; Valvatne et al., 2005; Dong & Blunt, 2007;
249 Joekar-Niasar et al., 2008; Andrew et al., 2014). Inevitably, the applicability of such
250 replicates of porous space is highly dependent on the porous media segmentation method
251 used for pore network extraction. Thus, a more realistic network extraction requires less

number of simplifications which will increase the accuracy by pore network modelling (Rabbani & Babaei, 2019).

Recently, watershed segmentation algorithm has been employed for pore network extraction from porous material images with complex geometries (Sheppard et al., 2004; Wildenschild & Sheppard, 2013; Rabbani et al., 2014, 2017b; Gostick, 2017; Rabbani & Salehi, 2017) which was used in this study (see Suppl. Material 1). This method utilises the geographical concept of watersheds to divide the pore-space of the porous material images into distinct pores and throats which could form an interconnected network of nodes and links (Rabbani et al., 2016, 2017a). Using the pore networks constructed, it will be possible to measure several properties of porous material (such as pore connectivity, pore radii, throat lengths and tortuosity) that provide quantified insights towards the changes of soil morphology when the aggregates are soaked in water. In this approach, it was assumed that throats are interfaces which connect adjacent pores, and they take up negligible volumes compared to pores (Rabbani & Babaei, 2019). To find the pore connectivity, which is the number of neighbour pore bodies connected to a single pore body, we scanned the segmented pore space image with a 3×3×3 sliding window. Each pore-body is labelled with a unique code, and from the codes of each neighbourhood voxels, the connectivity matrix (i.e. 1 for connected and 0 for no connection between pores) can be derived for an $N \times N$ matrix (N is the number of pores). A sample of extracted pore network image from aggregate from this study is provided in Suppl. Material 1.

Based on the definition of porous media tortuosity (Matyka et al., 2008), all path lengths are averaged and divided by the geometrical distance between the input and outlet set of pores. For defining inlet and outlet pores in the x-direction, we followed an ad hoc procedure. In x-direction, 5% of the pores with their first element of centre coordinates (positions along x-axis) smaller than the rest of pores are considered as inlet pores. Similarly, 5% of the pores

277 with the first element of centre coordinates larger than the rest of the pores are considered as
278 outlet pores. The same procedure was repeated for y and z directions. Knowing the positions
279 of inlet and outlet pores, we can find the shortest pathways in the network that connect these
280 pore bodies in each direction, thereby allowing to estimate directional tortuosity of networks
281 by dividing the shortest path to the geometrical distance (Matyka et al., 2008).

282 **2.4 Statistical analysis**

283 All the statistical analyses were performed using R version 3.4.0 (R Foundation for Statistical
284 Computing). The Post hoc Duncan test and the bootstrap correlations were performed using
285 the "DescTools" and "boot" packages, respectively.

286 For the first and second experiment, the differences in pore characteristics due to land use and
287 soil fractions was assessed by analysis of variance (ANOVA) coupled with Post Hoc Duncan
288 test, with land use and soil fractions as factors. When the normality and or homoscedasticity
289 of variances were not met, log transformation was applied. For the second experiment, the
290 effect of WDC on WSA (%) was assessed by ANOVA test.
291 The effect of wetting on pores and pore network characteristics was investigated using paired
292 Student's t-Test (as the same aggregate was measured before and after wetting). Spearman
293 correlation and linear regression between WSA and pores characteristics including the three
294 sizes of aggregates were performed for all or each land use. Due to the difference in the
295 number of replicates between WSA (n = 3) and pores characteristics (n = 8), we used
296 bootstrapping (a statistical procedure that resamples a single dataset to create thousands of
297 simulated samples to derive sample statistics) on the correlations (5000 bootstrap replicates).
298

299 **3. Results**

300 **3.1 PSD of Aggregates**

301 The image processing protocols followed in the study allowed visualisation and distribution
302 of different types of pores (closed, water holding and air space) within individual aggregates.
303 In Figure 1 (a-c), we present cross-sectional views of representative aggregates with different
304 types of pores (closed, water holding and air space pores) obtained from different land uses.
305 Overall, effective porosity followed the same trend as total porosity, and the effective
306 porosity was slightly smaller (1-2 %) than the total porosity as shown in Fig. 2 as it
307 represented the percentage of pores occupied by water and air and does not include closed
308 pore space. It was found that the total and effective porosities were significantly ($P = < 0.05$)
309 affected by land use and aggregate sizes. Total aggregates porosity, in particular from M and
310 L aggregates from the forest, was significantly higher (~4%) than the other two land uses.
311 The data also showed that both total and effective porosities of S were greater than those
312 compared to M and L and, were not influenced by the land use. In contrast to the total
313 porosity, the effective porosity of S, M and L were not significantly different for grassland.

314 Further portioning of total pore volume to percentages of closed, water and air holding pores,
315 showed closed pores tend to increase with the increase in aggregate size under arable land use
316 whereas the opposite trend was found in grassland and forest. Notably, for the S size class,
317 the percentage of closed pores was significantly higher in grassland and forest than in arable
318 land (uppercase letters, Fig. 3).

319 On the other hand, closed pore space in the L aggregates from the forest was significantly
320 lower than for the other land uses. Although there were no significant differences in the
321 distribution of water holding pore volumes between land uses for any specific aggregate size
322 class, in all cases, the proportion of water holding pores decreased with increasing aggregates

size (lowercase letters Fig. 3). However, the proportion of air space pores showed an opposite trend to the water holding pores between aggregates size, with an increasing proportion of air space pores with increasing aggregate size (lowercase letters, Fig. 3). Significant differences in air space pore volume between all aggregate sizes were found for forest and grassland. The air space pores also showed little difference between land uses; only the L size class was significantly higher in forest land use compared to arable (uppercase letters, Fig. 3).

3.2 Water stability of aggregates

Overall, the land use had the strongest effect on WSA, with grassland showing the highest proportion (~90%), followed by forest (~80%), while arable land showed low WSA (~20%) (upper case italic in Fig. 4). It appears from the data that the stability of aggregates tends to increase with aggregate size. The increase in WDCs number had a significant impact on arable and forest aggregates, however, the stability of grassland aggregates did not change significantly (lowercase letters in Fig. 4). The number or cycles had a stronger effect than the duration of the wetting. In the arable, WSA after nine short WDCs was significantly lower than with four short or long WDCs regardless of the macroaggregates size. For the forest, each size of macroaggregate was affected slightly differently by WDCs, with 1-2 mm showing the lowest WSA proportion after nine long WDCs, while for 2-5 mm it was after four long WDCs.

3.3 Effect of submergence on PSD

To demonstrate the resilience and stability of pore systems, PSD was examined before and after 24-hour submergence in water for two size groups of aggregates from grassland and forest. In general, the wetting for 24 hours in water of aggregates sizes 2-5 mm and 5-10 mm, did not significantly change the proportion of porosity, effective porosity, closed pores, water holding pores and air space pores in both grassland and forest aggregates (Fig. 5, 6).

347 Furthermore, this data was further split into different pore size groups (<30, 30-100 and >100
348 um) for M and L aggregates (Fig. 7). The proportion of these pore size groups did not show
349 any significant changes after 24 hours of wetting treatment (Fig. 7) for either M and L
350 aggregates from both grassland and forest. The M aggregates were significantly dominated
351 by 30-100 µm pores size, representing between 60-80 % of total pore space for grassland and
352 forest (lowercase letter, Fig. 7) whereas pores> 100 µm dominated in L aggregates indicating
353 a substantial macropore domain.

354 When we examined the changes in pore size, throat size, throat length, pore connectivity and
355 tortuosity in x, y and z directions (Table 2) it was evident that no statistically significant
356 changes occurred as a result of submergence, although the data showed that M samples had
357 experienced more change compared to L from grassland and forest. Overall, for both sets of
358 aggregate sizes, the changes of pore size, throat size and throat length remained below 10%.

359 Based on the PSD and WSA data obtained from these macroaggregates, we examined the
360 relationship between stability (WSA%) and the pore space in aggregates using bootstrapped
361 correlation (Spearman rank correlation, bootstrapped) and linear regression (Table 3 a & b).
362 The analysis was performed on the data from all land uses as well as for each land use (Table
363 3a). The regression (linear) could be performed only for arable land use as the data from
364 other land uses were not normally distributed (Table 3b). Values from these tables suggest
365 that there is a significant positive correlation between aggregate stability and three different
366 pore classes (closed, water and air holding) from individual land uses. When all data were
367 pooled, this was also true except for water holding pores. The data also showed significant
368 negative correlations between both porosity and effective porosity with stability for all land
369 use combined and also for arable and grassland individually. The regression analysis revealed
370 that for aggregates from arable soils, the pore system characteristics were significantly and
371 linearly related to WSA as shown in Table 3b.

4. Discussion

We acknowledge the fact that not all soil pores can be resolvable due to XMT resolution used in this study. Also, it must be noted that we scanned and processed L aggregates with a different resolution, which was mainly due to the technical limitation of the scanner we used. Using a lower resolution (20µm) may have underestimated of porosities in L aggregates. Therefore results must be interpreted carefully while comparing different sizes of aggregates because S & M were processed at the same resolution (10µm). Nevertheless, this difference does not pose an issue while comparing different land-use types for each aggregate size class. It may be noted that some previous works suggested that changing the resolution had minimal impact on total porosity as previously shown by De- Ville (2017, p 170) & De-Ville et al. (2018a).

Despite a recent increase in articles using imaging to study soil structure, there are only a handful of studies that focussed on aggregates. These studies include observation of 4-6.0 mm diameter aggregates at 14.6µm resolution (Kravchenko et al., 2011; Wang et al., 2012; Ananyeva et al., 2013), 1-3 mm aggregates at 4.4µm (Nunan et al., 2006), ~5 mm diameter aggregates with 3.2-5.4 µm resolution (Peth et al., 2008) and multiple aggregate sizes (0.25-0.425, 0.425-0.841, and 841-1.0 mm with 1 µm resolution (Bailey et al., 2013). This current study, by comparison, draws on a relatively larger sample size (69 aggregates) covering three land uses with 7-8 replicates from each group. Whereas most of the previous studies looked at the influence of tillage (conventional vs grassland/natural succession) on the aggregate structure (Peth et al., 2008; Kravchenko et al., 2011; Ananyeva et al., 2013) while Bailey et al. (2013) focussed their study only on grassland. A recent high resolution (1.51 µm) XMT imaging study demonstrated that the total pore volume in aggregates (between 0.71 -2 mm) was highest in grassland, followed by arable and fallow, demonstrating the impact of land use (Bacq-Labreuil et al. 2018). The main difference is while processing the images, we used a

complete aggregate volume rather than a region of interest (ROI) approach used in all previous studies. The problem of the ROI is it is user-defined (size, volume, position etc.) and it is most useful for materials with a relatively homogeneous structure, which is not the case for soil aggregates.

As Dexter (1988) proposed, each hierarchical order of aggregate excludes the pores between the particles of the next higher order. According to this hypothesis, the total porosity of aggregates will increase with an increase in size. Our data presented from three macroaggregates sizes suggest an opposite statistically-significant trend, especially for the arable land and grassland aggregate sizes S and M which were processed at the same resolution). Also, data from a previous study (Bailey et al., 2013), which used sub-millimetre sized aggregates (250-425; 425-841 and 841-1000 μm) did not reveal any particular trend between total pore volume (%) and aggregate size either. However, porosity obtained from these aggregates was much higher (17.2-54.9%) than we observed in our study (<10%) which is consistent with our results, which suggest that porosity may be likely to increase as the aggregate size decreases.

The characterisation of pore space also differed between studies. For instance, <15, 15-60 and >60μm pore size classifications were used to compare tillage systems in some studies (Kravchenko et al., 2011) whereas others used a simple histogram of pore volume distribution (Bailey et al., 2002; Peth et al., 2008). We have used three simple categories (closed, water holding and air spaces) of pores based on their potential role in water and air flow through the aggregates. The amount of resolvable pores in each category will depend on the image resolution. Closed pores or “blocked” pores (Dexter, 1988) which contain trapped air which will have no or limited contribution to the transport processes considered with our results show that such pores occupied approximately one-third of the total pore space available in aggregates. Hence, this pore volume was excluded for the calculation of effective

422 porosity, explaining why it was always lower than the total porosity. The observed pattern
423 suggests that in soils under arable land use, the closed pores increased with aggregate size
424 contrasting with grassland and forest. The reasons for this pattern is likely due to the
425 compaction from farm machinery because compaction leads to fragmentation of pores (i.e.
426 macropores will be changed to micropores) as demonstrated by Menon et al. (2015).

427 In our recent investigations (De-Ville et al., 2017, 2018) 50 µm threshold was used to
428 calculate water holding pores using XMT images based on the hypothesis proposed by Getter
429 et al. (2007) to improve retention performance of green roofs substrates. Small and medium-
430 sized aggregates in this study, for across the land uses contributed substantially (~30%) to the
431 water storage compared to the large aggregates (~40%). The opposite was true for air space
432 pores, which are critical for biota and drainage characteristics of the soils. Across the land
433 uses, we could see an increasing trend in air pore volume with the size of aggregate, whereas
434 the opposite was found for water holding pores. This is in agreement with the results from
435 Lipiec et al. (2007) in which they showed the existence of a more complex PSD and a
436 macropore domain in aggregates larger than >1 mm (Lipiec et al., 2007).

437 The breakdown of aggregates was explained by earlier studies (Yoder, 1936; Hénin S, 1938;
438 Dexter, 1988) through air-trapping and breakdown (slaking) as a result of the entry of water
439 into aggregates and it depends on the rate of wetting and water repellent properties of the
440 aggregates (Chenu et al., 2000; Cosentino et al., 2006; Bartoli et al., 2016). A meaningful
441 comparison of different wetting and drying cycles with previous studies is not very useful
442 here due to inconsistencies in the methods used to characterised the soil structure (Rabot et
443 al., 2018). Despite this, the impact on the WSA mass fraction of differently sized aggregates
444 by different WDCs suggested that it can impact the stability of arable and forest soil
445 aggregates compared to grassland aggregates, presumably due to higher SOC (Table 1)
446 compared to the other land uses. This experiment also revealed that the stability increased

447 with the size (except for grassland) and land use, regardless of the WDCs. Usually smaller
448 aggregates are supposed to be denser and stronger as proposed by earlier studies (Kemper &
449 Rosenau, 1984; Dexter, 1988; Elliott & Coleman, 1988; Oades, 1993; Fernández et al., 2010)
450 and it is possible that the stability of the large aggregates is influenced by other factors such
451 as Fe oxides and silt content, besides soil organic carbon (Regelink et al., 2015).

452 The relatively higher stability of grassland and forest aggregates motivated us further to the
453 development of the third hypothesis on the stability of the pore system. Although some subtle
454 changes in pore properties could be observed, in general, there was no statistically significant
455 difference in total, and effective porosities and different pore groups obtained from M and L
456 aggregates of forest and grassland suggested structurally resilient pore system in these
457 aggregates. The only exception is the water holding pore space of forest L aggregates. This
458 was not surprising because in our WDC experiment, we found some small decrease in the
459 stability of that forest aggregates compared to grassland aggregates. It is also important to
460 note that pore size, throat size and throat length are basic parameters and pore connectivity
461 and tortuosity are higher level parameters. Logically, the slight changes in basic parameters
462 could accumulate and lead to a more significant deviation in the higher level properties. For
463 example, a single additional throat between a cluster of pores could lead to an increase in
464 pore connectivity of all the cluster pores. That could be the reason behind the relatively
465 greater changes observed for connectivity and tortuosity.

466 The data and the correlations from this study demonstrate that the pore system in stable
467 aggregates undergoes relatively small and insignificant changes when submerged in water
468 and may, therefore, explain aggregate stability. We hypothesise that the pore networks in
469 stable aggregates act as conduits for transmission of fluids through without trapping the air
470 and thereby suppressing the build-up of air pressure inside an aggregate preventing it from
471 slaking, as previously proposed (Lipiec et al., 2007; Papadopoulos et al., 2009; Dal Ferro et

al., 2012). However, it is important to further investigate the underlying mechanisms contributing to the stability of the pores in aggregates. Several biotic (organic matter, soil fauna, roots, microbes) and abiotic factors (particle size distribution, clay minerals, exchangeable cations and sesquioxides) influence aggregate stability (Tisdall & Oades, 1982; Le Bissonnais, 1996; Amézketa, 1999; Chenu et al., 2000; Márquez et al., 2004; Bronick & Lal, 2005; Abiven et al., 2009; Regelink et al., 2015). Among this, soil organic matter is most influenced by the land use and hence, can be a highly influential factor in determining the aggregate stability (Yvan et al., 2012). One of such possibilities is the increased carbon accumulation in these pores, as shown by Ananyeva et al. (2011). In their study, they found that larger pores (100μm) are associated with higher carbon accumulation. Therefore, it can be further hypothesised that the organic carbon accumulated in larger pores provides enhanced stability to the pore walls and prevent them from collapse when submerged.

5. Conclusions

The main aim of this paper was to establish links between aggregate pore system characteristics and aggregate stability. We described PSD, and their stability of three different macroaggregate sizes (1-2; 2-5 and 5-10 mm) obtained from three different land uses (arable, grassland and forest). To explain the stability of aggregates, we evaluated the PSD and pore network changes in water stable aggregates before and after wetting. Our results show that smaller (1-2mm) aggregates have a greater degree of X-ray resolvable porosity compared to 2-5 mm or 5-10 mm sized aggregates. We found a significant influence of land use on PSD and water stability, in particular, grassland and forest aggregates were more stable than the arable aggregates. Using data derived from X-ray microtomography images, we demonstrated that the pore system of stable aggregates does not undergo significant changes upon continued submergence in water, indicating that a stable pore system is crucial for aggregate stability. The stability of aggregates has been recognised as a keystone factor

497 (Abiven *et al*., 2009) for soil fertility and physical resilience to external forces such as wind
498 or water; thus, this paper provides a new mechanistic understanding of WSA as an
499 appropriate indicator for soil quality and health.

500 **Acknowledgements**

501 Funding: This work was supported by SoilTrEC (Soil Transformations in European
502 Catchments) project in its 7th Framework Program (grant number 244118). Our sincere
503 thanks to Dr Taru Lehtinen, Ms Zijun Zhao and Mr George Reed for their help during the
504 different stages of this work. We also thank Dr Leslie Coulton who provided help at the
505 imaging facility in Sheffield.

506 **References**

507 Abiven, S., Menasseri, S. & Chenu, C. 2009. The effects of organic inputs over time on soil
508 aggregate stability - A literature analysis. Soil Biology and Biochemistry, **41**, 1–12.

509 Amézketa, E. 1999. Soil Aggregate Stability : A Review. Journal of Sustainable Agriculture,
510 **14**, 83–151.

511 Ananyeva, K., Wang, W., Smucker, A.J.M.J.M., Rivers, M.L.L. & Kravchenko, A.N.N.
512 2013. Can intra-aggregate pore structures affect the aggregate's effectiveness in
513 protecting carbon? Soil Biology and Biochemistry, **57**, 868–875.

514 Andrew, M., Bijeljic, B. & Blunt, M.J. 2014. Pore-scale imaging of trapped supercritical
515 carbon dioxide in sandstones and carbonates. International Journal of Greenhouse Gas
516 Control, **22**, 1–14.

517 Bacq-Labreuil, A., Crawford, J., Mooney, S.J., Neal, A.L., Akkari, E., McAuliffe, C., Zhang,
518 X., Redmile-Gordon, M. & Ritz K. 2018. Effects of cropping systems upon the three-
519 dimensional architecture of soil systems are modulated by texture. Geoderma. 332, 73-
520 83.

521 Bailey, V.L., McCue, L.A., Fansler, S.J., Boyanov, M.I., DeCarlo, F., Kemner, K.M. &
522 Konopka, A. 2013. Micrometer-scale physical structure and microbial composition of
523 soil macroaggregates. Soil Biology and Biochemistry, **65**, 60–68.

524 Bailey, V., Smith, J. & Bolton, H. 2002. Fungal-to-bacterial ratios in soils investigated for
525 enhanced C sequestration. Soil Biology and Biochemistry, **34**, 997–1007.

526 Banwart, S., Menon, M., Bernasconi, S.M., Bloem, J., Blum, W.E.H., De Souza, D.M.,
527 Davidsdotir, B., Duffy, C., Lair, G.J., Kram, P., Lamacova, A., Lundin, L., Nikolaidis,

528 N.P., Novak, M., Panagos, P., Ragnarsdottir, K.V., Reynolds, B., Robinson, D.,
529 Rousseva, S., de Ruiter, P., van Gaans, P., Weng, L., White, T. & Zhang, B. 2012. Soil
530 processes and functions across an international network of Critical Zone Observatories:
531 Introduction to experimental methods and initial results. Comptes Rendus - Geoscience,
532 **344**, 758–772.

533 Bartoli, F., Hallett, P.D. & Cerdan, O. 2016. Le Bissonnais, Y. 1996. Aggregate stability and
534 assessment of crustability and erodibility: 1. theory and methodology. European Journal
535 of Soil Science , 47, 425-437. European Journal of Soil Science, **67**, 5–10.

536 Le Bissonnais, Y. 1996. Aggregate stability and assessment of soil crustability and
537 erodibility : I . Theory and methodology. European Journal of Soil Science, **47**, 425–
538 437.

539 Banwart S.A., Nikolaidis N.P., Zhu Y.-G., Peacock C.L. & Sparks D.L. 2019. Soil functions:
540 connecting Earth's critical zone. Annual Review of Earth and Planetary Sciences (in
541 Press).

542 Blaud, A., van der Zaan, B., Menon, M., Lair, G.J., Zhang, D., Huber, P., Schiefer, J., Blum,
543 W.E.H., Kitzler, B., Wei, E.H., van Gaans, P. & Banwart, S. 2018. The abundance of
544 nitrogen cycle genes and potential greenhouse gas fluxes depends on land use type and
545 little on soil aggregate size. Applied Soil Ecology, **125**, 1–11.

546 Blunt, M.J. 2001. Flow in porous media - Pore-network models and multiphase flow. Current
547 Opinion in Colloid and Interface Science, **6**, 197–207.

548 Bronick, C.J.J. & Lal, R. 2005. Soil structure and management: a review. Geoderma, **124**, 3–
549 22.

550 Chenu, C., Le Bissonnais, Y. & Arrouays, D. 2000. Organic Matter Influence on Clay

551 Wettability and Soil Aggregate Stability. Soil Science Society of America Journal, **64**,
552 1479.

553 Cosentino, D., Chenu, C. & Le Bissonnais, Y. 2006. Aggregate stability and microbial
554 community dynamics under drying–wetting cycles in a silt loam soil. Soil Biology and
555 Biochemistry, **38**, 2053–2062.

556 Dal Ferro, N., Berti, A., Francioso, O., Ferrari, E., Matthews, G.P. & Morari, F. 2012.
557 Investigating the effects of wettability and pore size distribution on aggregate stability:
558 the role of soil organic matter and the humic fraction. European Journal of Soil Science,
559 **63**, 152–164.

560 De-Ville. 2017. Hydrological Performance Evolution of Extensive Green Roof Systems. PhD
561 thesis. University of Sheffield, U.K. Available online at
562 http://etheses.whiterose.ac.uk/17718/

563 De-Ville, S., Menon, M., Jia, X., Reed, G. & Stovin, V. 2017. The impact of green roof
564 ageing on substrate characteristics and hydrological performance. Journal of Hydrology,
565 **547**, 332–344.

566 De-Ville, S., Menon, M., Jia, X. & Stovin, V. 2018. A longitudinal microcosm study on the
567 effects of ageing on potential green roof hydrological performance. Water (Switzerland),
568 **10**.

569 De-Ville, S., Demirci, E., Frost, M. & Pattison, I. 2018a. Non-Invasive Property Analysis of
570 Heterogeneous Media Samples: How Small is Too Small?. EGU General Assembly
571 2018. Vienna, Austria, 8 – 13 April 2018.

572 Dexter, A.R. 1988. Advances in characterization of soil structure. Soil and Tillage Research,
573 **11**, 199–238.

574 Dong, H. & Blunt, M.J. 2007. Micro-CT imaging and pore network extraction. Department of
575 Earth Science and Engeneering, PhD Thesis Imperial College London.

576 Elliott, E.. 1986. Aggregate structure and carbon, nitrogen, and phosphorus in native and
577 cultivated soils. Soil Science Society of America Journal, **50**, 627–633..

578 Elliott, E.T. & Coleman, D.C. 1988. Let the soil work for us. Ecological Bulletins, 39:23-32.

579 Ferná ndez, R., Quiroga, A., Zorati, C., Noellemeyer, E., Argentina INTA, R.L.P., Covas, G.
580 & Argentina, L.P. 2010. Carbon contents and respiration rates of aggregate size fractions
581 under no-till and conventional tillage. Soil {&} Tillage Research, **109**, 103–109.

582 Getter, K.L., Rowe, D.B. & Andresen, J.A. 2007. Quantifying the effect of slope on extensive
583 green roof stormwater retention. Ecological Engineering, **31**, 225-231.

584 Gostick, J.T. 2017. Versatile and efficient pore network extraction method using marker-
585 based watershed segmentation. Physical Review E, **96**, 23307.

586 Hénin S. 1938. Etude physico-chimique de la stabilité structurale des terres. (At:
587 https://tel.archives-ouvertes.fr/tel-00752081/document. Accessed: 17/6/2018).

588 Joekar-Niasar, V., Hassanizadeh, S.M. & Leijnse, A. 2008. Insights into the relationships
589 among capillary pressure, saturation, interfacial area and relative permeability using
590 pore-network modeling. Transport in Porous Media, **74,** 201–219.

591 Kravchenko, N., Wang, N.W., Smucker, J.M., Rivers, M.L., Kravchenko, A.N., Wang,
592 A.N.W., Smucker, A.J.M. & Rivers, M.L. 2011. Long-term Differences in Tillage and
593 Land Use Affect Intra-aggregate Pore Heterogeneity. Soil Science Society of America
594 Journal, **75**, 1658.

595 Kemper, W.D., and R. Rosenau. 1984. Soil cohesion as affected by time and water content.
596 Soil Science Society of America Journal, **48,**1001–1006

597 Kibblewhite, M.G., Ritz, K. and Swift, M.J., 2007. Soil health in agricultural systems.
598 Philosophical Transactions of the Royal Society B: Biological Sciences, **363**, 685-701.

599 Lair, G.J., Zehetner, F., Hrachowitz, M., Franz, N., Maringer, F.-J. & Gerzabek, M.H. 2009.
600 Dating of soil layers in a young floodplain using iron oxide crystallinity. Quaternary
601 Geochronology, **4**, 260–266.

602 van Leeuwen, J.P., Djukic, I., Bloem, J., Lehtinen, T., Hemerik, L., de Ruiter, P.C. & Lair,
603 G.J. 2017. Effects of land use on soil microbial biomass, activity and community
604 structure at different soil depths in the Danube floodplain. European Journal of Soil
605 Biology, **79**, 14–20.

606 Lipiec, J., Walczak, R., Witkowska-Walczak, B., Nosalewicz, A., Słowińska-Jurkiewicz, A.
607 & Sławiński, C. 2007. The effect of aggregate size on water retention and pore structure
608 of two silt loam soils of different genesis. Soil and Tillage Research, **97**, 239–246.

609 Márquez, C.O., Garcia, V.J., Cambardella, C.A., Schultz, R.C. & Isenhart, T.M. 2004.
610 Aggregate-Size Stability Distribution and Soil Stability. Soil Science Society of
611 America Journal, **68**, 725–735.

612 Matyka, M., Khalili, A. & Koza, Z. 2008. Tortuosity-porosity relation in porous media flow.
613 Physical Review E - Statistical, Nonlinear, and Soft Matter Physics, **78**, 026306.

614 Menon, M., Jia, X., Lair, G.J., Faraj, P.H. & Blaud, a. 2015. Analysing the impact of
615 compaction of soil aggregates using X-ray microtomography and water flow
616 simulations. Soil and Tillage Research, **150**, 147–157.

617 Nunan, N., Ritz, K., Rivers, M., Feeney, D.S. & Young, I.M. 2006. Investigating microbial
618 micro-habitat structure using X-ray computed tomography. Geoderma, **133**, 398–407.

619 Oades, J.M. 1984. Soil organic matter and structural stability: mechanisms and implications

620 for management. Plant and Soil, **76**, 319–337.

621 Oades, J.M. 1993. The role of biology in the formation, stabilization and degradation of soil
622 structure. Geoderma, **56**, 377–400.

623 Papadopoulos, A., Bird, N.R.A., Whitmore, A.P. & Mooney, S.J. 2009. Investigating the
624 effects of organic and conventional management on soil aggregate stability using X-ray
625 computed tomography. European Journal of Soil Science, **60**, 360–368.

626 Peth, S., Horn, R., Beckmann, F., Donath, T., Fischer, J. & Smucker, A.J.M. 2008. Three-
627 Dimensional Quantification of Intra-Aggregate Pore-Space Features using Synchrotron-
628 Radiation-Based Microtomography. Soil Science Society of America Journal, **72**, 897.

629 R Foundation for Statistical Computing. R Core Team.

630 Rabbani, A., Assadi, A., Kharrat, R., Dashti, N. & Ayatollahi, S. 2017a. Estimation of
631 carbonates permeability using pore network parameters extracted from thin section
632 images and comparison with experimental data. Journal of Natural Gas Science and
633 Engineering, **42**, 85–98.

634 Rabbani, A., Ayatollahi, S., Kharrat, R. & Dashti, N. 2016. Estimation of 3-D pore network
635 coordination number of rocks from watershed segmentation of a single 2-D image.
636 Advances in Water Resources, **94**, 264–277.

637 Rabbani, A. & Babaei, M. 2019. Hybrid pore-network and Lattice-Boltzmann permeability
638 modelling accelerated by machine learning. Advances in Water Resources, **126**, 116–
639 128.

640 Rabbani, A., Baychev, T.G., Ayatollahi, S. & Jivkov, A.P. 2017b. Evolution of Pore-Scale
641 Morphology of Oil Shale During Pyrolysis: A Quantitative Analysis. Transport in
642 Porous Media, **119**, 143–162.

643 Rabbani, A., Jamshidi, S. & Salehi, S. 2014. An automated simple algorithm for realistic pore
644 network extraction from micro-tomography images. Journal of Petroleum Science and
645 Engineering, **123**, 164–171.

646 Rabbani, A. & Salehi, S. 2017. Dynamic modeling of the formation damage and mud cake
647 deposition using filtration theories coupled with SEM image processing. Journal of
648 Natural Gas Science and Engineering, **42**, 157–168.

649 Rabot, E., Wiesmeier, M., Schlüter, S. & Vogel, H.-J. 2018. Soil structure as an indicator of
650 soil functions: A review. Geoderma, **314**, 122–137.

651 Regelink, I.C., Stoof, C.R., Rousseva, S., Weng, L., Lair, G.J., Kram, P., Nikolaidis, N.P.,
652 Kercheva, M., Banwart, S. & Comans, R.N.J.J. 2015. Linkages between aggregate
653 formation, porosity and soil chemical properties. Geoderma, **247**–**248**, 24–37.

654 Rousseva, S., Kercheva, M., Shishkov, T., Lair, G.J., Nikolaidis, N.P., Moraetis, D., Kram,
655 P., Bernasconi, S.M., Blum, W.E.H., Menon, M. & Banwart, S.A. 2017. Soil Water
656 Characteristics of European SoilTrEC Critical Zone Observatories. Advances in
657 Agronomy, **142**, 29–72.

658 Sheppard, A.P., Sok, R.M. & Averdunk, H. 2004. Techniques for image enhancement and
659 segmentation of tomographic images of porous materials. In: Physica A: Statistical
660 Mechanics and its Applications, **339**, 145–151.

661 Six, J., Bossuyt, H., Degryze, S., Denef, K., Six, □ J, Bossuyt, H., Degryze, S., Denef, K.,
662 Six, J., Bossuyt, H., Degryze, S. & Denef, K. 2004. A history of research on the link
663 between (micro)aggregates, soil biota, and soil organic matter dynamics. Soil and
664 Tillage Research, **79**, 7–31.

665 Tisdall, J. & Oades, J. 1982. Organic matter and water-stable aggregates in soils. Journal of

soil science, **33**, 141–163.

Utomo, W. H., Dexter, a. R., UTOMO, W.H. & DEXTER, A.R. 1982. Changes in soil aggregate water stability induced by wetting and drying cycles in non-saturated soil. Journal of Soil Science, **33**, 623–637.

Valvatne, P.H., Piri, M., Lopez, X. & Blunt, M.J. 2005. Predictive pore-scale modeling of single and multiphase flow. In: Upscaling Multiphase Flow in Porous Media: From Pore to Core and Beyond, pp. 23–41.

Wang, W., Kravchenko, a. N., Smucker, a. J.M., Liang, W. & Rivers, M.L. 2012. Intra-aggregate Pore Characteristics: X-ray Computed Microtomography Analysis. Soil Science Society of America Journal, **76**, 1159.

Wildenschild, D. & Sheppard, A.P. 2013. X-ray imaging and analysis techniques for quantifying pore-scale structure and processes in subsurface porous medium systems. Advances in Water Resources, **51**, 217–246.

Yoder, R.E. 1936. A Direct Method of Aggregate Analysis of Soils and a Study of the Physical Nature of Erosion Losses1. Agronomy Journal, **28**, 337.

Yvan, C., Stéphane, S., Stéphane, C., Pierre, B., Guy, R. & Hubert, B. 2012. Role of earthworms in regenerating soil structure after compaction in reduced tillage systems. Soil Biology and Biochemistry, **55**, 93–103.

Zhou, H., Fang, H., Mooney, S. J., & Peng, X. 2016. Effects of long-term inorganic and organic fertilizations on the soil micro and macro structures of rice paddies. Geoderma, 266, 66-74.

689

690 **Figures Captions**

691 **Fig. 1.** (a-c). Example cross sectional view of (5-10 mm) aggregates from different land uses
692 with different types of pores obtained by processing X-ray microtomography images (a.
693 Arable, b. Grassland and c. Forest).

694 **Fig. 2.** Porosity and effective porosity (%) of soil aggregates sizes 1-2 (S), 2-5 (M) and 5-10
695 (L) mm from arable, forest and grassland soils. Mean and standard error are shown (n = 8,
696 except for 1 – 2 mm where n = 7). Different lowercase letters (a, b or c) show significant (P
697 < 0.05) differences between soil aggregates sizes for a specific land use. Different uppercase
698 letters (A, B or C) show significant (P < 0.05) differences between land use for a specific
699 soil aggregate size**.**

700 **Fig. 3.** Distribution of water holding, closed, and air space pores (%) of the total pore space
701 of soil aggregates sizes 1-2 (S), 2-5 (M) and 5-10 (L) mm from arable, forest and grassland
702 soils. Mean and standard error are shown (n = 8, except for 1 – 2 mm where n = 7). Different
703 lowercase letters (a, b or c) show significant (P < 0.05) differences between soil aggregates
704 sizes for a specific land use. Different uppercase letters (A, B or C) show significant (P <
705 0.05) differences between land use for a specific soil aggregate size.

706 **Fig. 4.** Distribution of water stable aggregates (%) of soil aggregates sizes 1-2 (S), 2-5 (M)
707 and 5-10 (L) mm from arable, grassland and forest soils under 4 short, 4 long and 9 short
708 wetting and drying cycles (WDCs). Mean and standard error are shown (n = 3). Different
709 minuscule letters show significant (P < 0.05) differences between WDCs for a specific soil
710 aggregate size and soil. Different capital letters show significant (P < 0.05) differences
711 between soil aggregate sizes for a specific soil and WDC. Different italic capital letters show
712 significant (P < 0.05) differences between soils for a specific soil aggregate size and WDC.

713 The minuscule and non-italic capital letters were not shown for grassland because no
714 significant differences were found.

715 **Fig. 5.** Porosity and effective porosity (%) of soil aggregates size a) 2-5 (M) & b) 5-10 (L)
716 mm from grassland and forest soils before and after 24h wetting in water. Mean and standard
717 error are shown (n = 3). ** indicate significant (P <0.01) difference between before and after
718 wetting.

719 **Fig. 6.** Distribution of water holding, closed, and air space pores of soil aggregates size a) 2-
720 5mm & b) 5-10 mm from forest and grassland soils before and after wetting 24h in water.
721 Mean and standard error are shown (n = 3). *** indicate significant difference

722 **Fig. 7.** Distribution of pore sizes (%) < 30 µm, 30-100 µm and > 100 µm in aggregates 2-5
723 mm and 5-10 mm from forest and grassland soils before and after wetting 24h in water. Mean
724 and standard error are shown (n = 3). Different lowercase letters (a, b or c) show significant
725 (P < 0.05) differences between soil pore size for a specific aggregates size, wetting state and
726 land use. Different uppercase letters (A, B or C) show significant (P < 0.05) differences
727 between land use for a specific soil aggregate size, pore size and wetting state. No significant
728 (P > 0.05) difference was found before and after wetting.

Table 1. Soil characteristics and soil aggregate size distribution of bulk soil samples on a dry mass basis at the time of sampling. Mean value ± one standard deviation (n = 3) are shown.

	Arable	Grassland	Forest
Location	48°09'N, 16°41'E	48°11'N, 16°44'E	48°08'N, 16°39'E
Water content (%)	11.3 ± 0.26	12.0 ± 0.26	17.1 ± 0.69
Soil pH (H_2O)	7.7 ± 0.14	7.4 ± 0.09	7.4 ± 0.17
Organic C (%)	2.4 ± 0.36	5.0 ± 0.60	3.8 ± 0.28
Total N (%)	0.13 ± 0.01	0.33 ± 0.04	0.25 ± 0.02
C_{org}/N	18.1 ± 1.83	15.0 ± 0.52	15.1 ± 1.02
$CaCO_3$ (%)	19.0 ± 1.90	21.1 ± 1.41	20.4 ± 0.62
Sand, 63-2000 µm (%)	32.7	8.2	22.5
Silt, 2-63 µm (%)	43.8	63.0	51.2
Clay, < 2 µm (%)	23.5	28.8	26.3
Soil Dry Aggregate Distribution (%)			
> 10 mm	37.3 ± 9.1	7.9 ± 2.4	11.9 ± 4.4
5.0 - 10.0 mm	14.6 ± 2.4	21.5 ± 2.0	18.3 ± 2.7
2.0 - 5.0 mm	20.5 ± 4.0	37.8 ± 3.6	31.2 ± 2.2
1.0 - 2.0 mm	11.8 ± 2.4	14.5 ± 0.5	23.1 ± 8.4
0.5 - 1.0 mm	6.4 ± 3.5	5.2 ± 0.4	5.9 ± 1.7
0.25 - 0.5 mm	7.1 ± 4.6	6.9 ± 0.1	7.5 ± 2.7
< 0.25 mm	1.9 ± 1.3	6.1 ± 0.7	2.0 ± 0.8

Table 2. Changes in pore network characteristics in grassland and forest 2-5 (M) and 5-10 (L) mm aggregates after 24 hours submergence.

	Grassland Aggregates				Forest Aggregates			
	M (n=3)		L (n =3)		M (n=3)		L (n=3)	
	Before Wetting	After Wetting	Before Wetting	After Wetting	Before Wetting	After Wetting	Before Wetting	After Wetting
Pore Radius (μm)	48.59±2.84	45.44±1.91	95.74±1.75	96.3±1.73	46.14±1.04	44.80±1.54	94.91±3.39	94.62±2.85
Pore throat radius (μm)	16.99±1.17	19.23±2.71	36.41±1.38	34.54±1.56	17.33±0.32	18.55±1.25	37.01±2.96	36.16±3.31
Pore throat length(μm)	200.12±37.02	212.36±29.12	428.24±35.26	419.89±24.12	161.79±4.46	170.99±10.28	363.21±20.20	346.08±4.00
Average pore connectivity	7.29±0.61	3.18±0.47	4.17±0.31	5.02±1.11	7.47±0.68	5.07±2.33	5.19±0.49	6.07±0.63
Tortuosity (x)	1.39±0.09	1.78±0.25	1.59±0.01	1.45±0.10	1.32±0.09	1.58±0.30	1.73±0.17	1.51±0.04
Tortuosity (y)	1.33±0.04	2.18±0.57	1.63±0.08	1.61±0.09	1.35±0.12	1.63±0.32	1.45±0.02	1.46±0.13
Tortuosity (z)	1.44±0.06	2.07±0.50	1.50±0.08	1.61±0.11	1.36±0.04	1.50±0.20	1.41±0.03	1.41±0.08

Table 3 (a) Bootstrap statistics of Spearman correlation coefficient between WSA method 1 and pores characteristics. Significant correlation are shown in bold ($P < 0.001$).

Landuse	Bootstrap statistics	Porosity	Effective porosity	Closed pores	Water holding pores	Air space pores
All LU	Original value	**-0.25**	**-0.24**	**0.29**	0.10	**0.23**
	bias	0.0031	0.0011	0.0005	-0.0004	-0.0013
	Std error	0.080	0.076	0.076	0.073	0.070
	95% Conf Int	-0.40; -0.09	-0.38; 0.08	0.13; 0.43	-0.04; 0.25	0.08; 0.36
Arable	Original value	**-0.51**	**-0.51**	**0.77**	**0.65**	**0.75**
	bias	0.0079	0.0073	-0.0089	-0.010	-0.0098
	Std error	0.110	0.113	0.070	0.090	0.074
	95% Conf Int	-0.69; -0.25	-0.69; -0.24	0.59; 0.87	0.43; 0.79	0.56; 0.86
Grassland	Original value	**-0.46**	**-0.35**	**0.74**	**0.61**	**0.78**
	bias	0.0032	0.0032	-0.0060	-0.0077	-0.0066
	Std error	0.105	0.116	0.060	0.079	0.055
	95% Conf Int	-0.64; -0.22	-0.56; -0.09	0.59; 0.83	0.44; 0.75	0.63; 0.86
Forest	Original value	-0.07	0.08	**0.90**	**0.88**	**0.90**
	bias	-0.0017	-0.0002	-0.0082	-0.0091	-0.0090
	Std error	0.157	0.160	0.023	0.029	0.022
	95% Conf Int	-0.36; 0.25	-0.24; 0.39	0.86; 0.94	0.82; 0.93	0.86; 0.94

Table 3 (b). Bootstrap statistics of linear regression r^2 between WSA method 1 and pores characteristics. Significant correlation are shown in bold ($P < 0.001$).

	Bootstrap statistics	Porosity	Effective porosity	Closed pores	Water holding pores	Air space pores
Arable	Original value	**0.36**	**0.36**	**0.15**	**0.60**	**0.39**
	bias	0.0015	0.0016	0.012	-0.0019	0.0057
	Std error	0.088	0.088	0.086	0.080	0.112
	95% Conf Int	0.18; 0.52	0.18; 0.53	0.02; 0.34	0.42; 0.74	0.16; 0.60

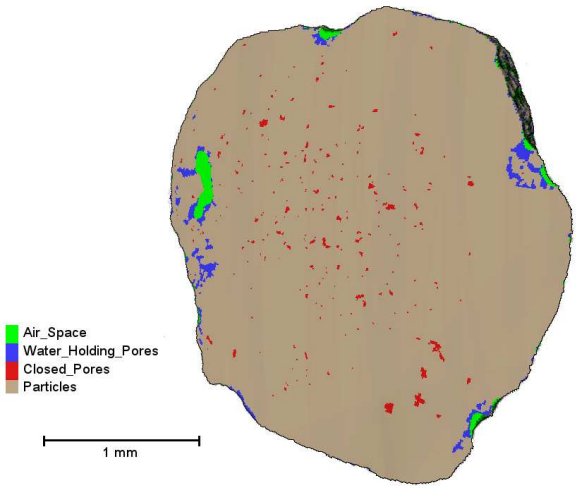
Air_Space
Water_Holding_Pores
Closed_Pores
Particles
1 mm

(a)

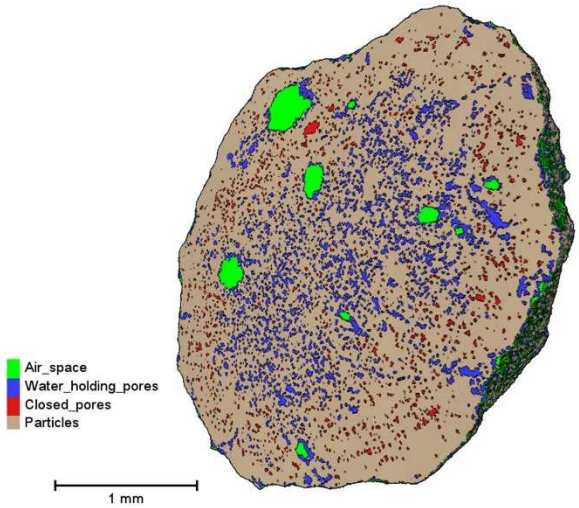
Air_space
Water_holding_pores
Closed_pores
Particles
1 mm

(b)

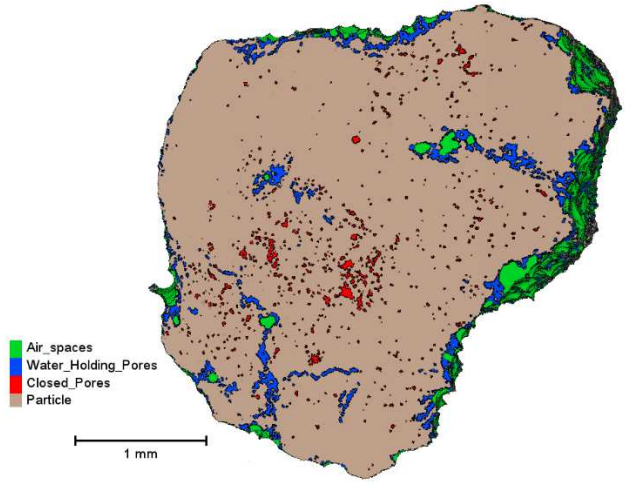
Air_spaces
Water_Holding_Pores
Closed_Pores
Particle
1 mm

(c)

Figure 1.

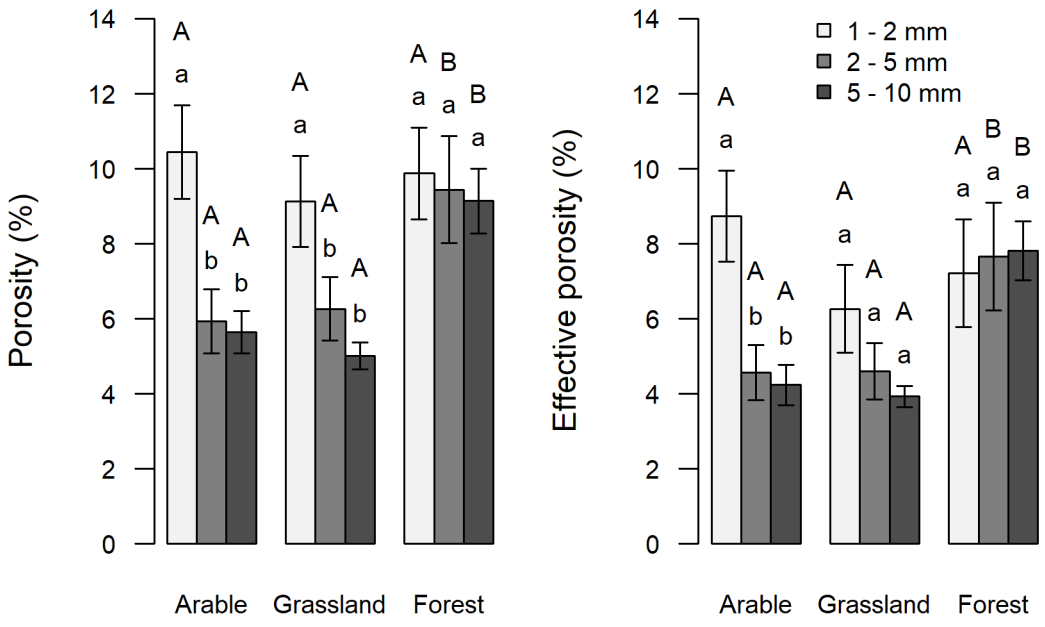
Porosity (%)
Effective porosity (%)
1 - 2 mm
2 - 5 mm
5 - 10 mm
Arable
Grassland
Forest

Fig. 2.

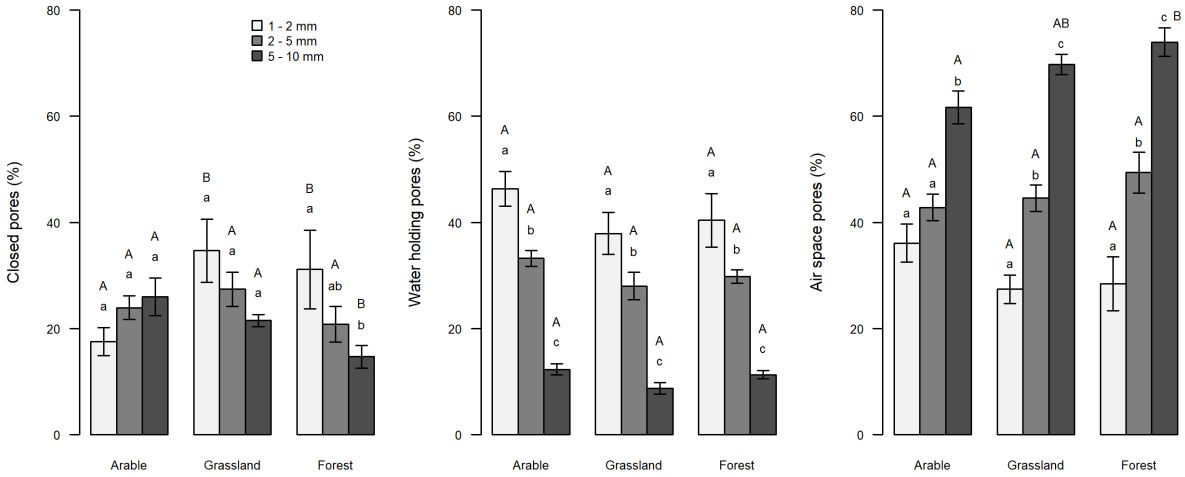
Closed pores (%)
Water holding pores (%)
Air space pores (%)
1 - 2 mm
2 - 5 mm
5 - 10 mm
0
20
40
60
80
Arable
Grassland
Forest

Fig. 3.

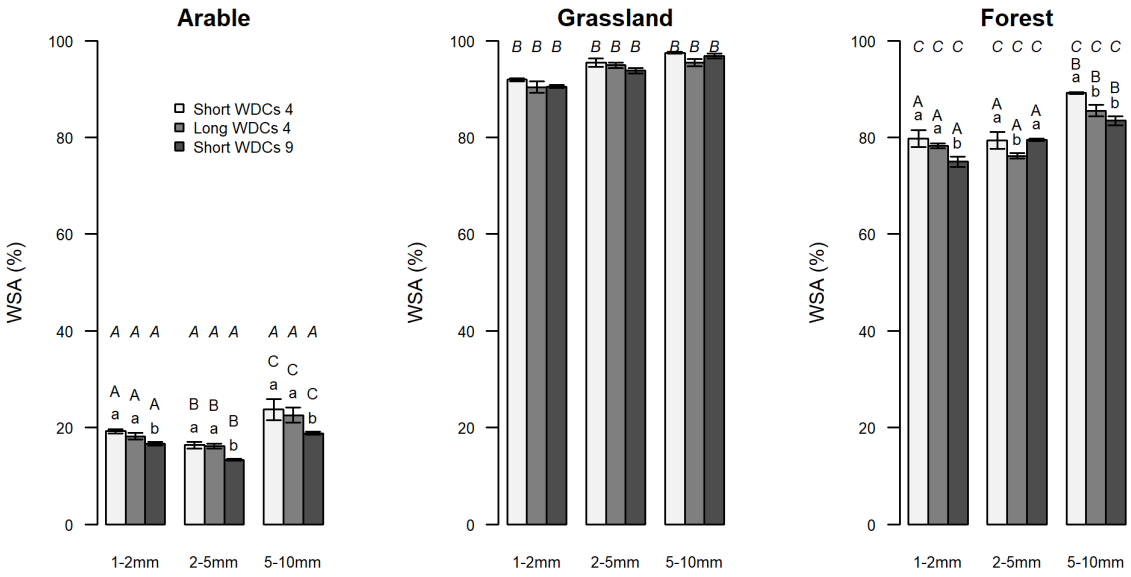
Arable
Grassland
Forest
Short WDCs 4
Long WDCs 4
Short WDCs 9
WSA (%)
0
20
40
60
80
100
1-2mm
2-5mm
5-10mm

Fig. 4.

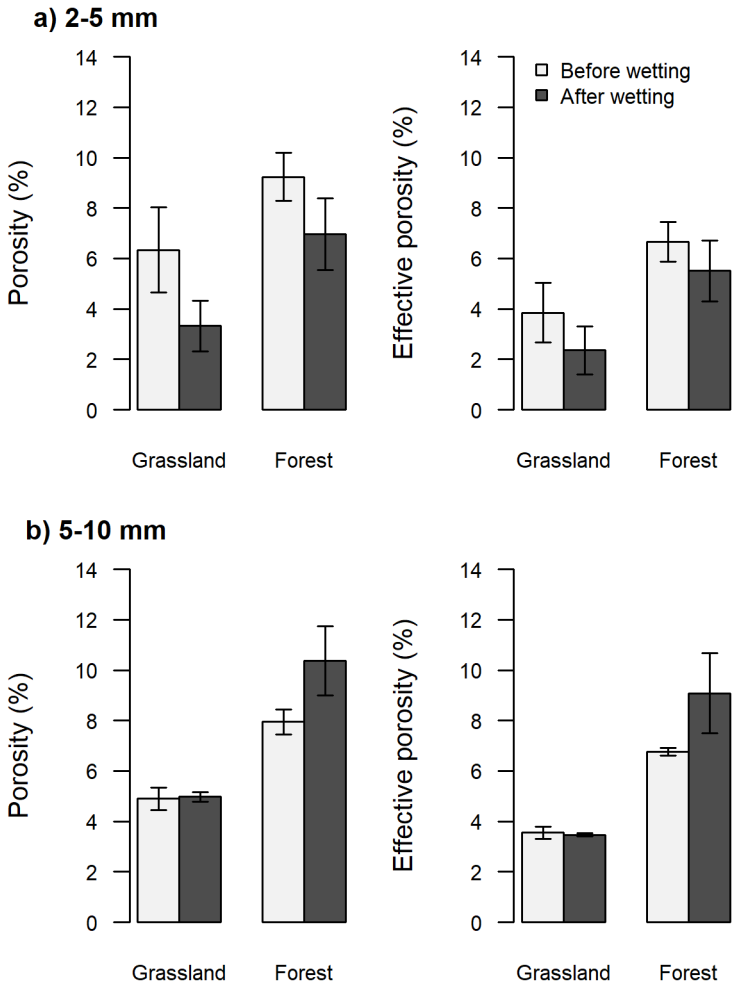
a) 2-5 mm
Porosity (%)
Effective porosity (%)
Before wetting
After wetting
Grassland
Forest
b) 5-10 mm
Porosity (%)
Effective porosity (%)
Grassland
Forest

Fig. 5.

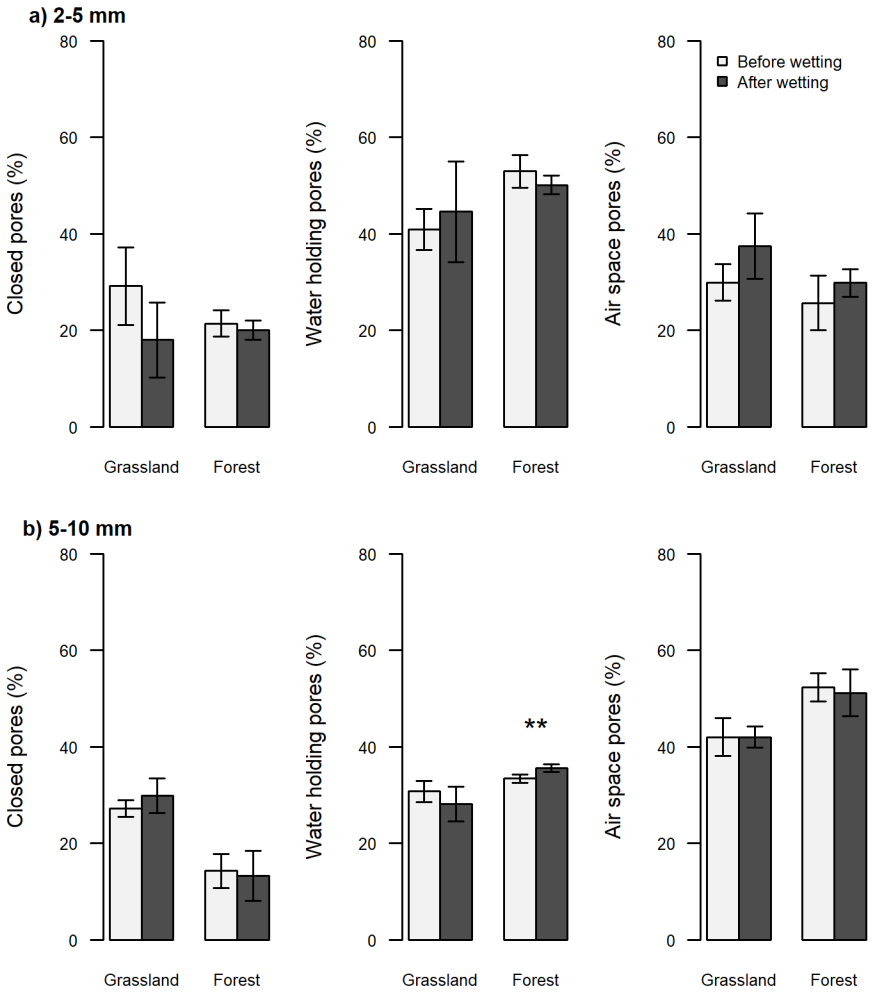
a) 2-5 mm
b) 5-10 mm
Closed pores (%)
Water holding pores (%)
Air space pores (%)
Before wetting
After wetting
Grassland
Forest
**
0
20
40
60
80

Fig. 6.

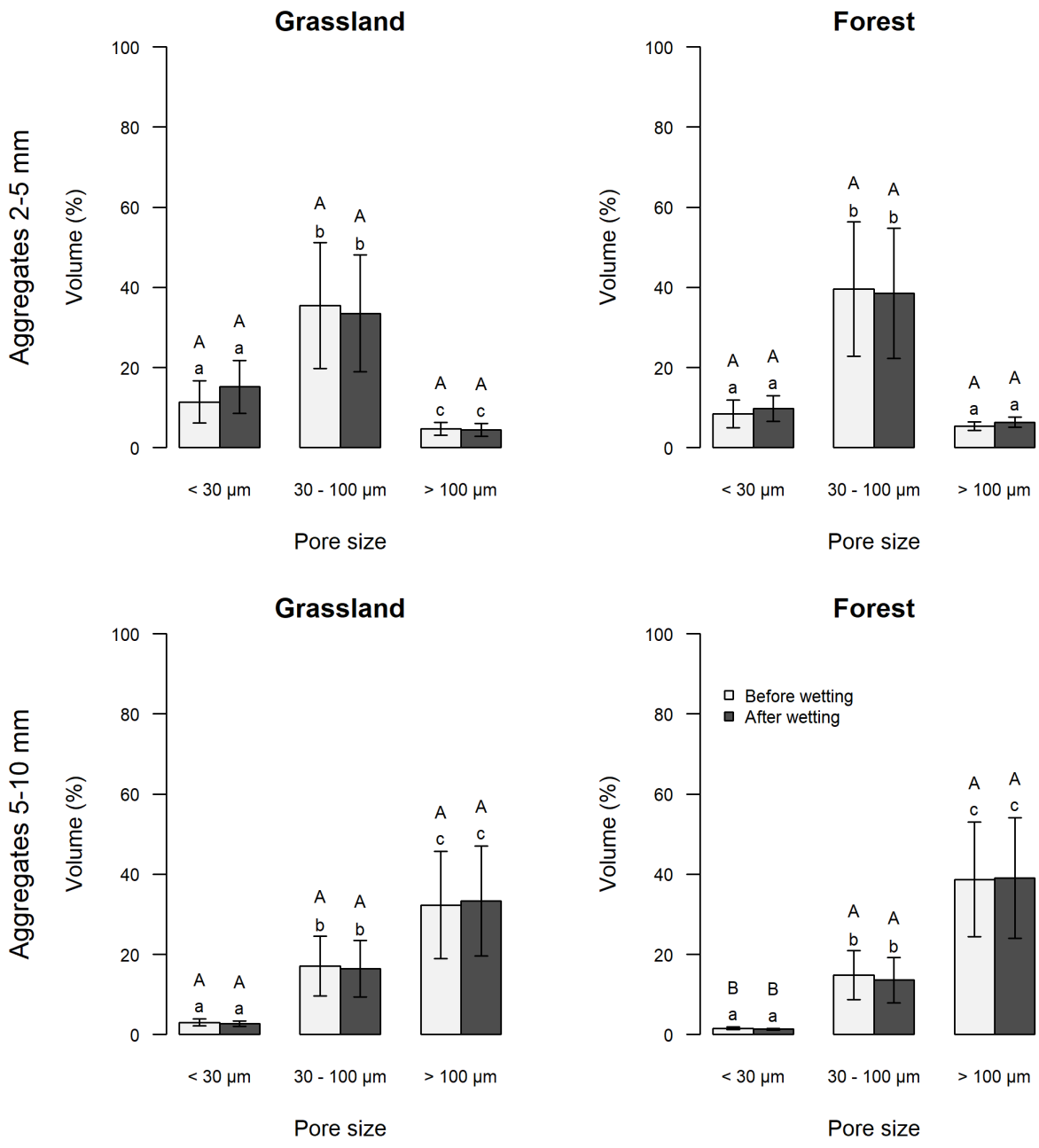
Grassland
Forest
Aggregates 2-5 mm
Aggregates 5-10 mm
Volume (%)
Pore size
< 30 µm
30 - 100 µm
> 100 µm
Before wetting
After wetting

Fig. 7.

Supplementary Material 1 for image processing and pore network extraction

1. Image acquisition settings

Beam hardening and partial volume effects can reduce the quality of the images. In order to avoid the beam hardening effect, metal filters are used in the micro-CT scanner to pre-harden the beam. Also, in order to reduce the partial volume effect, the rotation steps are selected to be as low as 0.700 degree. Other imaging settings are included in Table A.1.

Table A.1. Imaging settings used to scan aggregates of different sizes in this study

Image acquisition settings	Aggregate size (mm)	
	1-2 or 2-5	5-10
Source voltage (kV)	49	70
Source current (uA)	200	141
Camera pixels	1048 x 2000	
Imager rotation	0.32	
Pixel size	5.01	10.02
Object to source (mm)	46.755	93.465
Camera to source (mm)	214.136	
Al Filter 0.5 mm	Yes	
Image format	TIFF	
Exposure (ms)	295 or 590	
Rotation step (deg)	0.700	
360 rotation	Yes	
Median filter	On	
Flat field correction	On	
Geometrical correction	On	
Scanning trajectory	Round	

2. Image processing steps (Performed using Avizo 9.0.1)

Initially, 16bit Grayscale raw images obtained from the several different CT scans carried out were converted to 8bit images to reduce the computational requirements for processing. The resultant greyscale images obtained were then filtered using a 3D median filter (Avizo 9.0.1) with a neighbourhood of 6 and 1 iteration to reduce image noise. Next, a global thresholding algorithm based on the histogram of the greyscale image was applied to delineate soil mineral particles (higher attenuation values) from their corresponding background (lower attenuation values). Afterwards, to define the **closed pores** within aggregates, a 3D fill holes algorithm with a neighbourhood of 6 was applied which sealed off the isolated pores, these delineated pores were then delineated by subtracting the result from the defined particle mask. To define the **water holding pores**, a ball closing algorithm with a diameter of 50µm (equivalent number of pixels) was used to seal off all pores connected to the surface with a diameter smaller than 50µm. The resultant output mask was then subtracted from the particle mask with the defined closed pores being removed leaving only the required sized pores delineated. Lastly, to define the **air pores**, the particle mask was closed using a disc closing algorithm with a kernel size large enough to fully seal all the large and small internal pores (around 2.5% of the particle length). The disc instead of the ball was used as it reduced aggregate surface space inclusions by about 20%. The air pores were then delineated by subtracting particles, closed and water holding pores from the output mask leaving the air spaces. The steps followed for the above-described process are summarised in Supp. Figure 1 & 2 below.

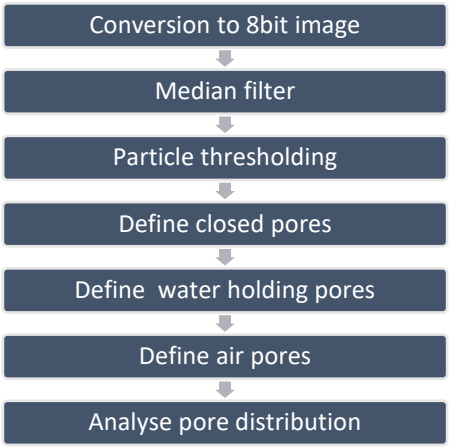

Supp. Fig. 1. Steps involved in image processing of aggregates

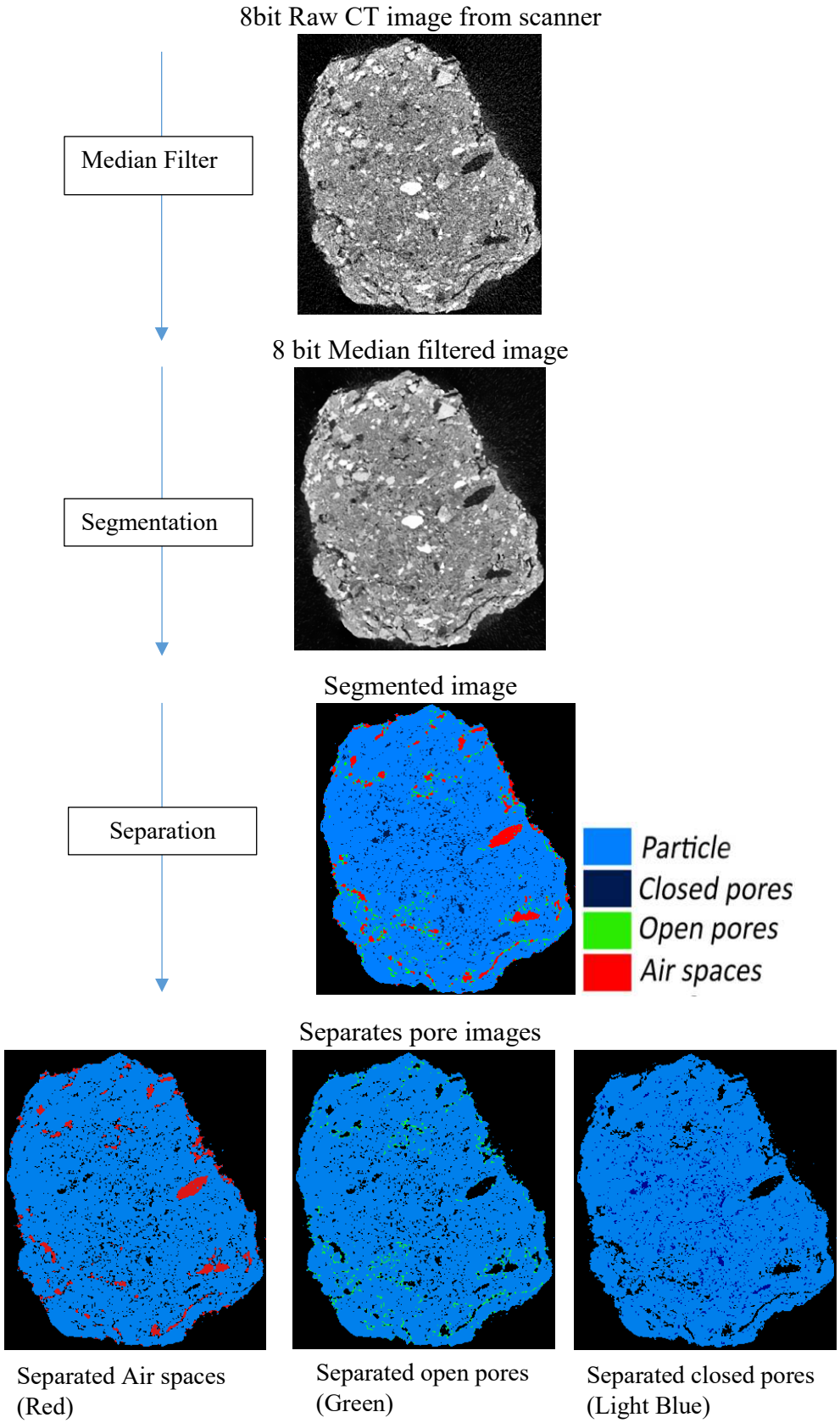

Supp. Fig. 2. Visualisation of major steps involved in image processing of aggregates

3. Pore Network Extraction steps

Binarised images of soil aggregates were analysed to extract the pore network model using watershed segmentation algorithm. We used an in-house code to define what part of the network is composed of pore-bodies and how they are connected to each other by pore-throats. In this approach, initially, we performed distance transform on 3-D binarised images and applied Gaussian filtering to avoid over-segmentation of the porous media. Then watershed transform was applied on the images that create several growing nuclei at the centre of the pores in which distance value is locally maximized. These nuclei keep growing based on the distance values until they touch a nucleus from the neighbouring pore. Then the touching voxels were recorded as pore-throats. The process continued until the whole volume of the void space be filled with the growing nuclei. Then, we subtracted the pore-throat voxels from the void geometry and applied morphological labelling to address each detected pore which was by then isolated from its neighbours. In the next step, with a 3×3×3 sliding window we browsed the whole labelled geometry to find and label the connections between each pair of pores as pore-throats. Finally, we measured the size of each pore-throat and thus, the network was fully extracted. See suppl. Figure 3 illustrates the steps in the described workflow and example pore network extracted is given in Suppl. Figure 4.

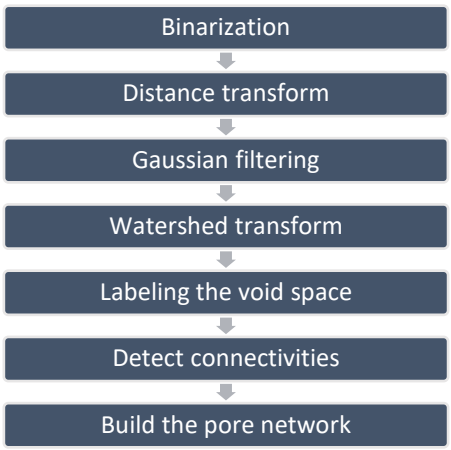

Suppl. Figure 3. Pore network extraction process using watershed segmentation algorithm

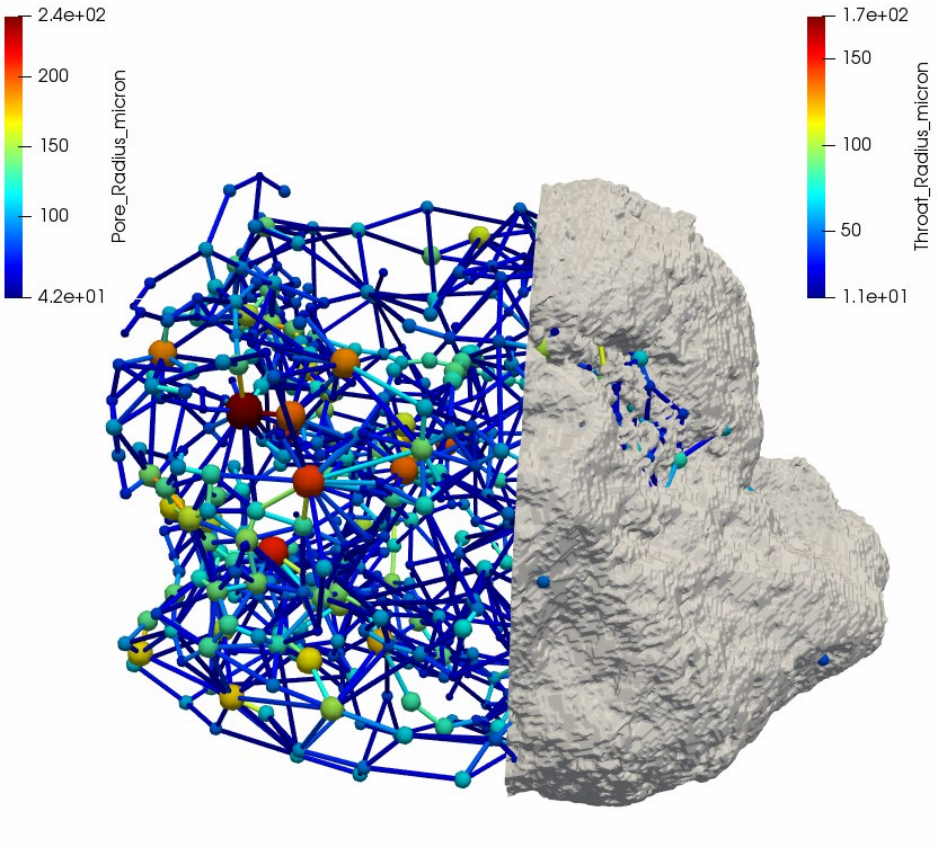

Suppl. Figure 4. Inside view of pore and throat sizes of an grassland aggregate (5-10 mm) based on the extracted pore network.